PCCP

Physical Chemistry Chemical Physics

Accepted Manuscript

Volume 19
Number 1
7 January 2017
Pages 1-896

PCCP

Physical Chemistry Chemical Physics

rsc.li/pccp

ISSN 1463-9076

PAPER
H.-P. Loock et al.
Determination of the thermal, oxidative and photochemical degradation rates of scintillator liquid by fluorescence EEM spectroscopy

ROYAL SOCIETY OF CHEMISTRY

This is an Accepted Manuscript, which has been through the Royal Society of Chemistry peer review process and has been accepted for publication.

Accepted Manuscripts are published online shortly after acceptance, before technical editing, formatting and proof reading. Using this free service, authors can make their results available to the community, in citable form, before we publish the edited article. We will replace this Accepted Manuscript with the edited and formatted Advance Article as soon as it is available.

You can find more information about Accepted Manuscripts in the Information for Authors.

ROYAL SOCIETY OF CHEMISTRY

rsc.li/pccp

Journal Name

ARTICLE TYPE

Photo-induced 6π-electrocyclisation and cycloreversion of isolated dithienylethene anions[†]

Jack T. Buntine,[a] Eduardo Carrascosa,[b] James N. Bull,[c] Giel Muller,[a] Ugo Jacovella,[d] Christopher R. Glasson,[e] George Vamvounis,[f] and Evan J. Bieske[*a]

The diarylethene chromophore is commonly used in light-triggered molecular switches. The chromophore undergoes reversible 6π-electrocyclisation (ring closing) and cycloreversion (ring opening) reactions upon exposure to UV and visible light, respectively, providing bidirectional photoswitching. Here, we investigate the gas-phase photoisomerisation of *meta-* (*m*) and *para-* (*p*) substituted dithienylethene carboxylate anions (DTE⁻) using tandem ion mobility mass spectrometry coupled with laser excitation. The ring-closed forms of *p*-DTE⁻ and *m*-DTE⁻ are found to undergo cycloreversion in the gas phase with maximum responses associated with bands in the visible ($\lambda_{max} \approx 600$ nm) and the ultraviolet ($\lambda_{max} \approx 360$ nm). The ring-open *p*-DTE⁻ isomer undergoes 6π-electrocyclisation in the ultraviolet region at wavelengths shorter than 350 nm, whereas no evidence is found for the corresponding electrocyclisation of ring-open *m*-DTE⁻, a situation attributed to the fact that the antiparallel geometry required for electrocyclisation of *m*-DTE⁻ is energetically disfavoured. This highlights the influence of the carboxylate substitution position on the photochemical properties of DTE molecules. We find no evidence for the formation in the gas phase of the undesirable cyclic byproduct, which causes fatigue of DTE photoswitches in solution.

Introduction

Photoisomerisation plays a key role in many biological processes and technological applications, including in the visual transduction cycle in animals and as phototriggers in photopharmacology where the absorption of light in the bio-optical window can activate drug molecules.[1–5] One appealing strategy for understanding the intrinsic behaviour of molecular photoswitches is to study the molecules in the gas phase, an isolated environment, and compare the photochemistry with studies in solution where the environment plays a role. Data gathered for molecules in the gas phase can normally be compared in a straightforward manner with theoretical predictions.

Common classes of molecular photoswitches include the

fulgides, azobenzenes, spiropyrans, and diarylethenes (DAEs).[6,7] Ideal photoswitch molecules should be thermally stable at room temperature, exhibit rapid photoswitching response with high quantum yield, and resist fatigue after repeated photoswitching cycles.[7] DAEs satisfy most of these criteria and offer other advantages including simple syntheses, capacity to be grafted to other molecules (e.g. enzymes or polymers) and a high propensity for reversible/bi-directional photoisomerisation with different colours of light (photochromism).[6–8] DAEs have been developed for various applications including optics and photonics, and show promise for photoswitching of bioactive molecules or enzyme activity.[6,7,9]

The photoswitching function of DAEs (Fig. 1a) involves 6π-electrocyclisation (ring closing) and cycloreversion (ring opening) reactions upon exposure to light, respectively. The photo-induced 6π-electrocyclisation follows the Woodward-Hoffmann rules, involving a conrotatory cyclisation of a hexatriene system giving anti-configured stereochemistry. The photo-induced cycloreversion process also proceeds through a conrotatory mechanism to give the ring-open form. Note that in solution the ring-open isomer can exist as two interconvertible geometric forms, antiparallel and parallel (Fig. 1a); only the antiparallel conformation has the correct orientation of the hexatriene system for photo-induced electrocyclisation.[7,10] Introducing long, sterically cumbersome alkyl groups to the photoactive carbon atoms on the thiophene rings restricts the ring-open isomer to the antiparal-

[a] School of Chemistry, The University of Melbourne, Parkville, Victoria 3010, Australia; E-mail: evanjb@unimelb.edu.au

[b] Bruker Daltonics GmbH & Co. KG, Fahrenheitstrasse 4, 28359 Bremen, Germany.

[c] School of Chemistry, Norwich Research Park, University of East Anglia, Norwich NR4 7TJ, United Kingdom.

[d] Université Paris-Saclay, CNRS, Institut des Sciences Moléculaires d'Orsay, 91405 Orsay, France.

[e] Environmental Research Institute, School of Science, University of Waikato, Tauranga, 3110, New Zealand.

[f] College of Science and Engineering, James Cook University, Townsville, Queensland 4811, Australia.

[†] Electronic Supplementary Information (ESI) available. See DOI: 10.1039/b000000x/
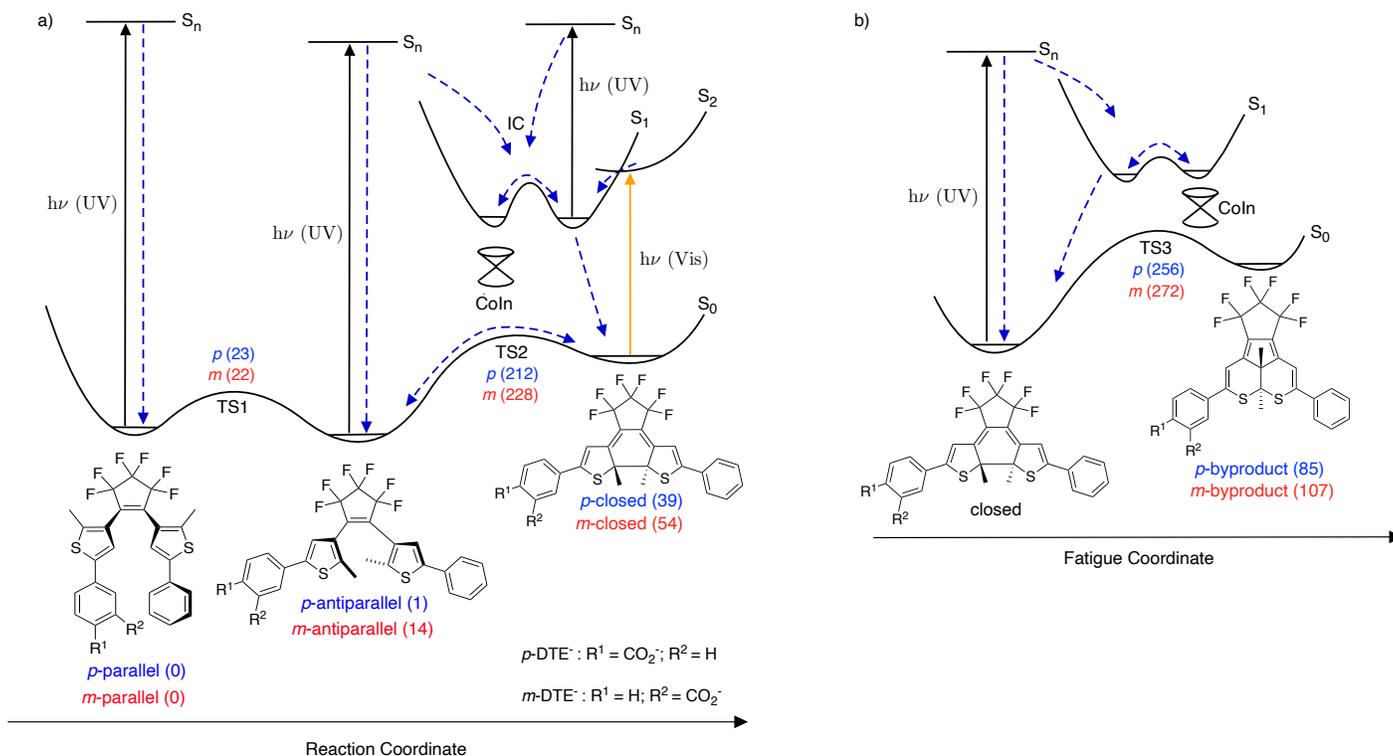
Fig. 1 Potential energy surfaces for the dithienylethene (DTE) anions investigated in this work. Energies for minima and transition states were calculated at the ωB97X-D/aug-cc-pVDZ level of theory. Relative energies (in kJ/mol) are reported in parentheses. Photoexcitation is represented by full arrows; IC=internal conversion pathways (represented by blue, dashed arrows); CoIn=conical intersection; TS=transition state.

lel structure and consequently increases the cyclisation quantum yield in solution.[11,12] The quantum yield for the cycloreversion reaction is generally lower than the cyclisation yield, presumably due to the existence of a barrier on the singlet S_1 excited-state surface, but normally increases with the introduction of electron-withdrawing substituents,[13,14] while electron-donating substituents tend to decrease the yield significantly.[15,16]

Many DAE photoswitch molecules in condensed phases show formation of a photostable cyclic byproduct following prolonged exposure of the ring-closed isomer to UV light.[17,18] In contrast, visible light does not lead to degradation. The structure of the byproduct was first elucidated by Irie and coworkers using mass spectrometry and X-ray crystallography.[17,19] Time-dependent HPLC studies established that the byproduct was formed from the ring-closed isomer following exposure to UV light. It was also found that the byproduct has a very similar absorption spectrum to that of its ring-closed precursor. Interestingly, in the single-crystalline phase, DAEs exist exclusively in the antiparallel arrangement and do not degrade to the cyclic byproduct upon exposure to UV light.[20,21] Formation of the byproduct is undesirable and is the main source of fatigue in DAE photoswitches (Fig. 1b), although it remains uncertain whether the degradation is an inherent feature of the molecule or depends on the solvent environment.

A desire to understand the photoisomerisation dynamics and absorption properties of DAEs has prompted numerous solution-based experiments[17,19,22–33] and theoretical investigations,[33–42] including studies on the formation mechanism for the byprod-

uct.[33,43–47] For the cyclisation and cycloreversion reactions, theory[39,41,42,48–50] has established the involvement of a conical intersection seam between the ground state S_0 and first excited singlet state S_1. Studies of the photochemical formation mechanism for the byproduct are limited, although a theoretical investigation by Mendive-Tapia *et al.* suggests involvement of a S_1/S_0 conical intersection seam in the non-adiabatic decay from the singlet S_1 state.[44] Although the functionalisation of DAEs, for example by substituting the stilbene phenyl rings with thiophene functional groups [i.e. dithienylethenes (DTEs)], can enhance the photoisomerisation quantum yield, it can also exacerbate fatigue.[17,19] However, DAE systems containing benzothiophene moieties have been shown to be one of the most fatigue-resistant derivatives,[51,52] and formation of the byproduct has been suppressed by using a triplet sensitiser to induce cyclisation through a triplet state.[45]

Gas-phase photochemistry of molecular photoswitches provides a basis for interpreting their photoswitching behaviour in solution and better understanding photoswitch-solvent interactions. To our knowledge, there are only two prior investigations of neutral DTE molecules in the gas phase. One study observed fluorescence spectra for the ring-open isomer in a supersonic free jet,[53] and the other used femtosecond time-resolved photoelectron spectroscopy to measure excited-state lifetimes.[54] In the current study we apply photoisomerisation action (PISA) spectroscopy to investigate the isomer-specific photochemistry of two charged DTE systems in the gas phase. The PISA spectroscopy technique couples ion mobility spectrometry (IMS) with laser

spectroscopy, allowing investigation of selected DTE isomers. In drift tube IMS, charged isomers (e.g. *E* and *Z* isomers, deprotomers, or ring open/closed structural isomers) are propelled through a buffer gas by an electric field and are separated based on their drift speeds, which depend on their collision cross sections (CCSs) with the buffer gas. In PISA spectroscopy, a target isomer is selected in a primary IMS stage and exposed to tunable laser light, with resulting photoisomers separated in a second IMS stage. Monitoring the photoisomerisation response as a function of laser wavelength gives a gas-phase action spectrum. The PISA spectroscopy technique has been used previously to study a range of molecular transformations in the gas phase, including *E-Z* photoisomerisation,[55–58] linkage photoisomerisation,[58] electrocyclisation[59] and photo-induced intramolecular proton transfers.[60] In this study we use the PISA approach to investigate the effect of substitution pattern on the photoisomerisation of carboxylated DTE molecules. The investigation also provides insights into the role solvent plays in photoisomerisation.

Experimental methods

Experiments were performed using a tandem ion mobility mass spectrometer shown in Fig. 2 that has been described previously.[61,62] Synthesis of *p*-DTE and *m*-DTE is described in the ESI. Briefly, gas-phase anions were generated through electrospray ionisation from a solution of the target molecule dissolved in methanol ($\approx 10^{-5}$ mol/L) with trace NH_3. A radio frequency-driven ion funnel (IF1) radially gathered and confined the electrosprayed ions, after which an ion gate (IG1) injected 100 μs packets of ions at 40 Hz into the first stage of the drift region (IMS1). The ions were propelled through N_2 buffer gas (≈ 6 Torr) by an electric field (44 V/cm) where they were separated spatially and temporally based on their collision cross-sections with the gas. Extended isomers have larger collision cross-sections and travel more slowly than smaller, more compact ions. After the ions traversed the drift region, they were collected by a second ion funnel (IF2) and passed through a differentially pumped chamber containing an octupole ion guide and quadrupole mass filter (QMF) before striking an ion detector. A plot of ion signal against arrival time at the detector corresponds to an arrival time distribution (ATD) and exhibits peaks associated with different isomers. The mobility resolution of the instrument for singly-charged anions, $t/\Delta t$, is typically 80-90.[62]

Photoisomerisation of the DTE$^-$ anions was probed by operating the instrument in tandem mode. A Bradbury-Nielsen electrostatic ion gate (IG2) situated midway along the drift region was opened for 100 μs at an appropriate delay to select the desired target isomer. The mobility-selected ions were intercepted by a single 10 ns pulse of light from a tunable optical parametric oscillator (OPO, EKSPLA NT342B). The resulting photoisomers or photofragments were then separated in the second stage of the drift tube (IMS2). The instrument was operated such that alternate ion packets were intercepted by light, so that the photoresponse could be assessed through the difference between the light-on and light-off ATDs, the photoaction ATD. PISA spectra were obtained by monitoring the photoisomer yield as a function of OPO wavelength. The PISA spectroscopy measurements were performed with a light fluence of <0.5 mJ/cm^2/pulse to minimise multiphoton absorption and dissociation processes. The maximum photoresponse corresponded to conversion of $<8\%$ of the ring-closed structures to the ring-open structures at wavelengths of 615 and 590 nm for *p*-DTE$^-$ and *m*-DTE$^-$, respectively. It should be noted that although the PISA spectra are normalised with respect to laser power, the relative intensities of the visible and UV bands are somewhat uncertain as the OPO changes range at 410 nm and the beam profile is slightly different in the visible (410-700 nm) and UV regions (300-410 nm).

Measured collision cross sections (Ω_m) were derived from the measured arrival times, t, of the ions adjusted for the time they spend in the octupole, t_{oct}, and QMF, t_{quad}, where $t = t_d + t_{oct} + t_{quad}$.[63] The time the ions spend in the octupole and QMF is short (≈ 0.2 ms) compared to their transit times through the drift region, t_d (17–20 ms).

Theoretical methods

To support the PISA experiments, electronic structure calculations for *p*-DTE$^-$ and *m*-DTE$^-$ isomers were performed using the Gaussian 16.B01 software package.[64] Geometry optimisations, harmonic vibrational frequencies and isomerisation transition-state geometry searches were performed at the ωB97X-D/aug-cc-pVDZ level of theory.[65,66]

Calculated collision cross sections were computed using the Ion Mobility Software (IMoS) 2.0 program suite[67] with the trajectory method parametrised for N_2 buffer gas at 298 K. Input charge distributions were computed at the ωB97X-D/aug-cc-pVDZ level of theory during the course of the geometry optimisation and vibrational frequency calculation using the Merz+Singh+Kollman scheme to reproduce the electric dipole moments.[68,69] Sufficient trajectories were computed such that calculated values had standard deviations of ± 1 Å^2.

Results and discussion

In solution, ring-open DTEs are present in antiparallel and parallel conformations (Fig. 1a).[7,10] A molecule in the antiparallel conformation is photoreactive as it possesses a suitable geometry for 6π-electrocyclisation, whereas the geometry of a molecule in the parallel conformation is unsuitable for electrocyclisation. Calculated relative energies (ωB97X-D/aug-cc-pVDZ level of theory) for the ground-state minima and transition states for the two target DTE molecules in the gas phase are summarised in Fig. 1a and b. The parallel ring-open isomer is predicted to be the minimum energy form for both *p*-DTE$^-$ and *m*-DTE$^-$ molecules. For *m*-DTE$^-$, the parallel structure is more stable than the antiparallel structure (by 14 kJ/mol), due to non-covalent interactions between the –CO$_2^-$ charge-tag and the aromatic ring system on the adjacent arm (see Fig.2c SI). For *p*-DTE$^-$, similar non-covalent interactions between the –CO$_2^-$ charge-tag and the aromatic ring system are not structurally possible, so that the parallel and antiparallel forms are almost isoenergetic.

Arrival time distributions (ATDs) for *p*-DTE$^-$ and *m*-DTE$^-$ are shown in Fig. 3a and b, respectively. The ATDs were recorded for DTE$^-$ ions from electrosprayed methanolic solutions of the synthesised ring-open isomers, with the solutions shielded from room
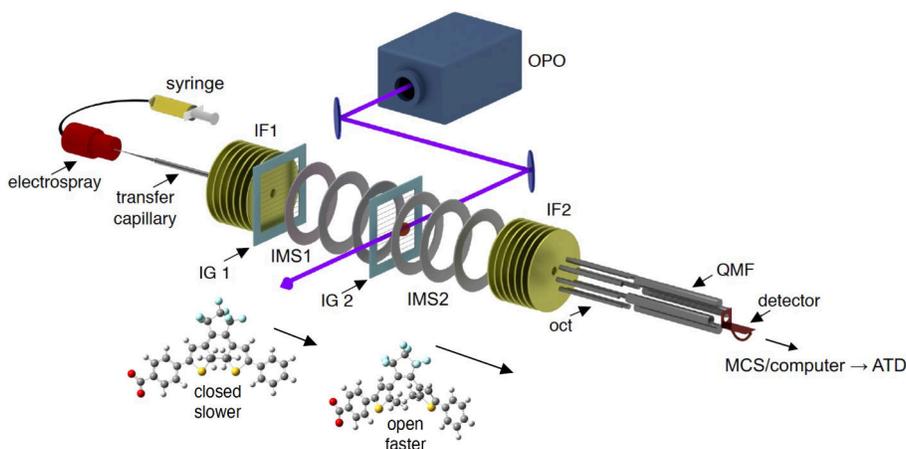
Fig. 2 Schematic illustration of the tandem ion mobility spectrometer coupled with laser excitation. IF1 = first ion funnel, IG1 = first ion gate, IMS1 = ion mobility stage 1, IG2 = second ion gate, IMS2 = ion mobility stage 2, IF2 = second ion funnel, oct = octupole, QMF = quadrupole mass filter, MCS = multichannel scaler, and OPO = optical parametric oscillator.
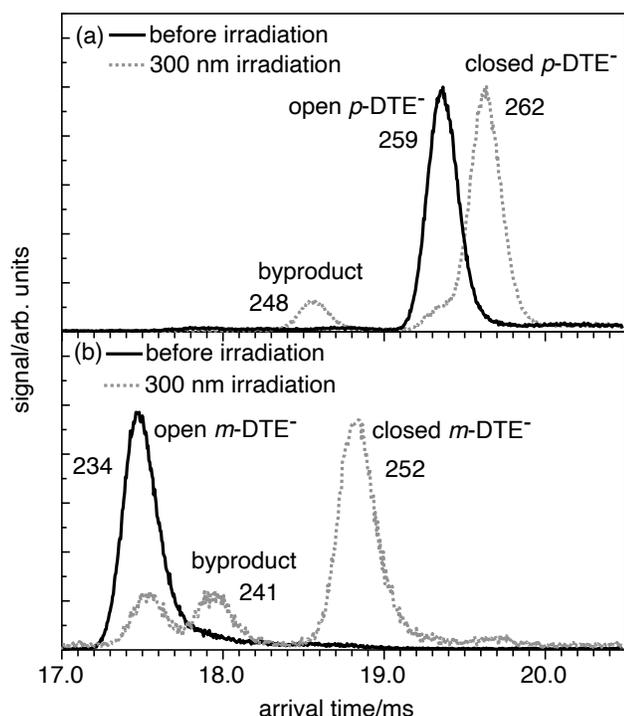

Fig. 3 ATDs for p-DTE$^-$ and m-DTE$^-$ in N$_2$ buffer gas, with and without irradiation at 300 nm. (a) ATDs for ring-open and ring-closed p-DTE$^-$. (b) ATDs for ring-open and ring-closed m-DTE$^-$. The ATD peaks tentatively assigned to the byproduct are identified. Measured collision cross sections for each ATD peak are given in Å^2.

light (clear solutions), and also for electrosprayed methanolic solutions that were irradiated with 300 nm light for several minutes (blue solutions). Comparison of the ATDs allows assignment of the major peak for the solutions protected from light to the ring-open isomer, and the major peak for the solutions irradiated with 300 nm light to the ring-closed isomer, with the minor peak tentatively assigned to the cyclic degradation product formed through the process shown in Fig. 1(b).[19] The photoconversion between

ring-open and ring-closed forms of DTE$^-$ is well known in solution.[7]

The low TS1 barrier of 23 kJ/mol separating the parallel and antiparallel structures of ring-open p-DTE$^-$ means that the two forms should rapidly interconvert in the drift tube on a shorter time scale than their transit time, giving rise to a single, time-averaged ATD peak.[70] This is consistent with the ATD shown in Fig. 3(a), which shows a single peak that can be assigned to the ring-open isomer. As discussed later, p-DTE$^-$ molecules in the antiparallel conformation travelling in this packet are photoactive and undergo 6π-electrocyclisation when exposed to UV light. For ring-open m-DTE$^-$, rapid interconversion between the parallel and antiparallel structures is also expected in the drift tube due to the low TS1 barrier of 22 kJ/mol (see Fig.1) giving a single, time-averaged ATD peak as shown in Fig. 3(b). However, ions in this packet will mostly have the more stable parallel structure, which will not undergo electrocyclisation, consistent with the absence of any photoisomerisation response when this ion packet was irradiated at 300 nm (see below).

The peak assignments for the ring-open and ring-closed isomers of p-DTE$^-$ and m-DTE$^-$ are generally consistent with collision cross sections calculated using the IMoS 2.0 program package based on structures determined using DFT (ωB97X-D/aug-cc-pVDZ level of theory). Measured (Ω_m) and calculated (Ω_c) CCSs for p-DTE and m-DTE anions are summarised in Table 1. As explained above, both the parallel and antiparallel conformers should contribute to the ring-open ATD peaks, and therefore the effective CCS will be a weighted average of the CCSs for the two conformers. For p-DTE$^-$, the measured CCS for the closed form is around 1.2% larger than the CCS of the open form, agreeing with calculations which predict the CCS of the closed form is 1.7% larger than that of the open form. For m-DTE$^-$, the measured CCS for the closed form is 7.7% larger than the CCS for the open isomer, comparable to the 7.5% difference between the calculated CCSs for the closed isomer and the parallel conformer of the open isomer (expected to be the main form of the open isomer in the ion packet).

Table 1 Measured and calculated CCSs (Ω) for p-DTE and m-DTE anions in N_2 buffer gas (units Å^2). Absolute errors in the measured collision cross sections are estimated as $\pm 20\,\text{Å}^2$, with relative errors being somewhat lower, $\pm 3\,\text{Å}^2$.

	CCSs	
species	Ω_m (Å^2)	Ω_c (Å^2)
p-DTE$^-$		
open (antiparallel)	-	251
open (parallel)	-	225
open (average CCS)	259	238
closed	262	242
byproduct	248	245
m-DTE$^-$		
open (antiparallel)	-	250
open (parallel)	-	227
open (average CCS)	234	239
closed	252	244
byproduct	241	243

For both p-DTE$^-$ and m-DTE$^-$, the calculated CCS of the byproduct is larger than expected if the assignments of the byproduct ATD peaks are correct. At this stage we do not have an explanation for this discrepancy. Proving that the minor peaks observed in Figs. 3(a) and (b) are indeed associated with the byproducts shown on the right hand side of Fig. 1 might be accomplished using HPLC separation of the constituents of the irradiated solutions, followed by structural characterisation, probably using NMR. Following this, the purified byproduct samples for p-DTE$^-$ and m-DTE$^-$ could be introduced into the ion mobility mass spectrometry instrument to check that their arrival times indeed correspond to the minor peaks observed in Figs. 3(a) and (b), respectively.

Having assigned the main ATD peaks, we now consider the photoisomerisation of the DTE$^-$ ions in the gas phase. Photoaction ATDs (the difference between light-on and light-off ATDs) for ring-open and ring-closed isomers of p-DTE$^-$ recorded at different wavelengths are shown in Fig. 4(a-d). Measurements for the ring-open p-DTE$^-$ isomer (Fig. 4(a)) at 300 nm are consistent with photoconversion of the antiparallel form to the ring-closed isomer with a minor fraction of the molecules photodissociating through loss of CO_2 (confirmed by tuning the quadrupole mass filter to the $-CO_2$ photofragment). An overall reduction in ion signal accompanying exposure of the ring-open p-DTE$^-$ isomer to 300 nm light is presumably due to photodetachment as the photon energy (4.13 eV) exceeds the calculated adiabatic electron affinity (AEA) of 3.77 eV. The ring-open p-DTE$^-$ isomer shows no discernible photoresponse at wavelengths longer than 350 nm consistent with calculations (see below) and measurements in solution. For the ring-closed p-DTE$^-$ isomer, the photoaction ATDs show evidence for formation of the ring-open isomer in the visible and UV ranges (Fig. 4(b)&(c)) and also for loss of CO_2 and F atoms in the UV range (Fig. 4(c)). Note that measurements of photoproduct yield as a function of light fluence at 615 nm suggests that photoisomerisation involves absorption of a single photon (Fig. S3(a) in the ESI).
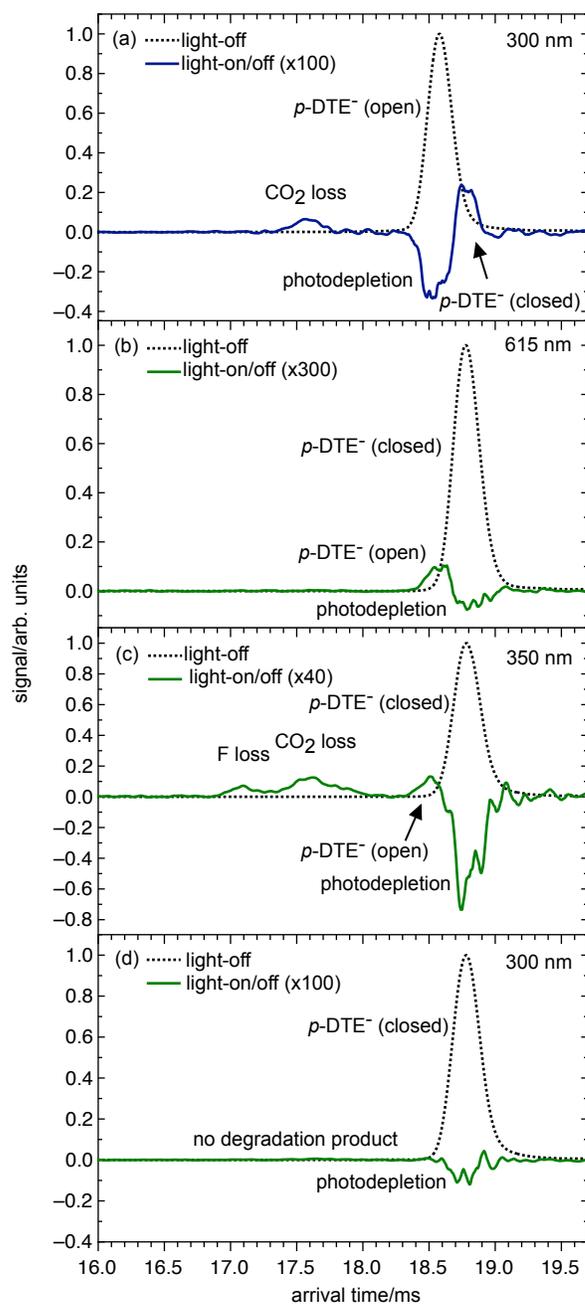

Fig. 4 Photoaction ATDs for photoisomerisation of p-DTE$^-$. (a) ring-open isomer irradiated at 300 nm showing formation of the ring-closed isomer, (b) ring-closed isomer at irradiated 615 nm showing cycloreversion, (c) ring-closed isomer irradiated at 350 nm showing cycloreversion and photodissociation signals corresponding to loss of CO_2 and an F atom, respectively, and (d) ring-closed isomer irradiated at 300 nm with evidence for photodetachment but not for byproduct formation. All photoaction ATDs were recorded with the QMF set to transmit all ions. Note, because the mobility-selected ions are intercepted with light midway through the drift region (after IMS1), the photoisomer signals appear between the ATD peaks of the two isomeric forms that are separated over the entire drift region (IMS1+IMS2).

We now consider the photoresponse of the m-DTE$^-$ isomers in the gas phase. First we note that no photoisomerisation response was observed for the ring-open m-DTE$^-$ isomer over the

300-700 nm range, presumably because in the gas phase the ring-open isomer exists mainly in the more stable parallel conformation, which, due to its unfavourable geometry, is unable to cyclise (Fig. 1(a)). This is apparent in the photoaction ATD for the ring-open m-DTE$^-$ isomer at 300 nm (Fig. 5(a)), which shows no evidence for formation of the ring-closed isomer, whose peak should appear at $\approx$18 ms, but which does show evidence for photo-induced CO_2 loss and for photodetachment (the calculated AEA is 4.03 eV for ring-open m-DTE$^-$). In contrast, as shown in Fig. 5(b), the ring-closed isomer does convert to the ring-open isomer when exposed to 590 nm light. Measurements for the photoisomer yield as a function of light fluence at 590 nm presented in the ESI (Fig. S3(b)) suggest that the process involves absorption of a single photon. Between 300 and 400 nm, cycloreversion of the ring-closed m-DTE$^-$ isomer occurs in competition with photodissociation (CO_2 and F loss) (Fig. 5(c)). Exposure of ring-closed m-DTE$^-$ to 300 nm light (Fig. 5(d)) results in the formation of a small amount of the ring-open isomer and the CO_2 and F-atom dissociation products but with most of the photodepletion signal presumably due to electron detachment (the calculated AEA is 3.96 eV for ring-closed m-DTE$^-$).

There is no evidence in the photoaction ATDs for ring-open and ring-closed isomers of p-DTE$^-$ or m-DTE$^-$ shown in Figs. 4 and 5 for formation of the species tentatively assigned to the byproduct following exposure to visible or UV light. This is perhaps not surprising given that measured quantum yields for byproduct formation for similar DAE molecules in solution are low, with an upper limit of 0.02.[7,45] We estimate that the relative quantum yield for byproduct formation in the gas phase would need to exceed 0.1 for its peak to be apparent in the photoaction ATDs under single photon absorption conditions.

Photoisomerisation action (PISA) spectra for ring-open and ring-closed p-DTE$^-$ isomers are shown in Fig. 6(a). The PISA spectrum for 6π-electrocyclisation of ring-open p-DTE$^-$ has an onset at $\approx$360 nm and probably reaches a maximum at a wavelength just below 300 nm. The PISA spectrum resembles the solution absorption spectrum (methanol, pH>7), and is consistent with time-dependent density functional theory (TD-DFT) ωB97X-D/aug-cc-pVDZ calculations which predict a strong transition for the ring-open isomer at 286 nm (oscillator strength, f=0.85). The PISA spectrum for cycloreversion of ring-closed p-DTE$^-$ shown in Fig. 6(a) exhibits a band spanning the 450–700 nm range, peaking at $\approx$615 nm, and a band of comparable intensity extending over the 320–415 nm range, peaking at $\approx$365 nm. The UV band is likely associated with two UV transitions apparent in the solution absorption spectrum (370 and 383 nm). The visible band in the absorption spectrum of p-DTE$^-$ in solution is blue-shifted $\approx$20 nm compared with the band in the gas-phase PISA spectrum. This shift can be interpreted as arising from a diminished solvent stabilisation of the molecule in the excited state compared to the ground state. Overall, the PISA spectrum of ring-closed p-DTE$^-$ is consistent with TD-DFT calculations that predict transitions at 547 nm (f=0.51), 335 nm (f=0.38) and 321 nm (f=0.37). It should be remarked that in the UV region, photodissociation through loss of CO_2 and F become competitive with photoisomerisation of ring-closed p-DTE$^-$ so that the total photoproduct
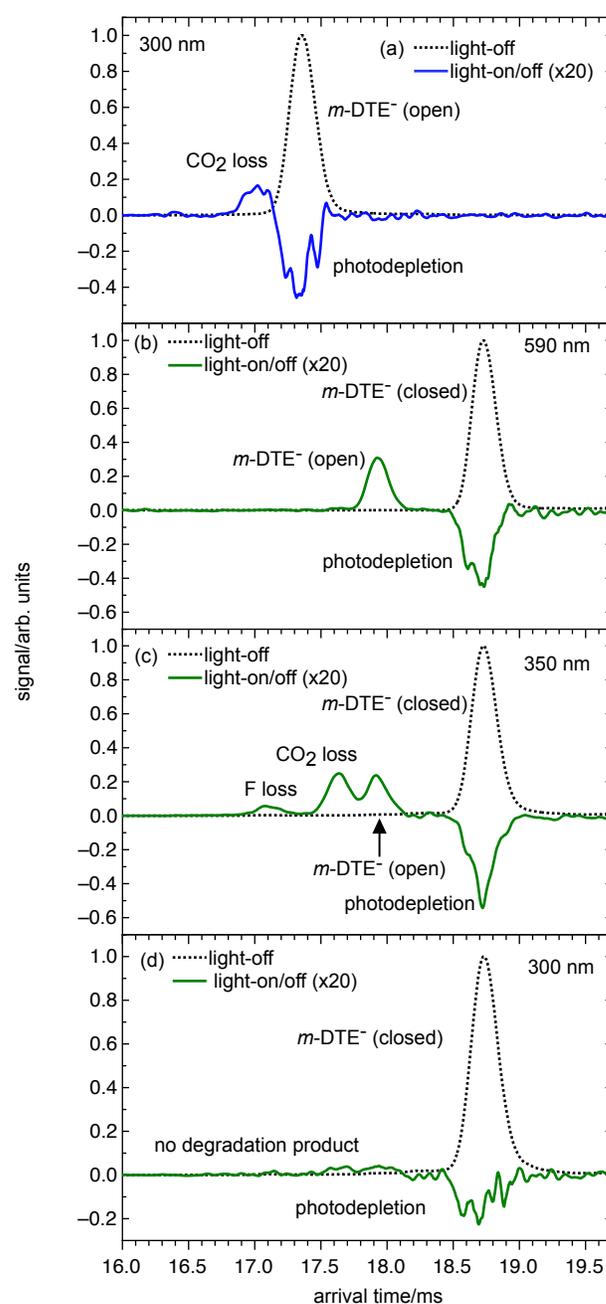

Fig. 5 Photoaction ATDs for m-DTE$^-$. (a) ring-open isomer irradiated at 300 nm showing CO_2 loss, (b) ring-closed isomer irradiated at 590 nm showing cycloreversion, (c) ring-closed isomer irradiated at 350 nm showing cycloreversion and photodissociation signals corresponding to the loss of CO_2 and a fluorine atom, respectively, and (d) ring-closed isomer irradiated at 300 nm with evidence for photodetachment but not for byproduct formation. All photoaction ATDs were recorded with the QMF set to transmit all ions.

yield at the peak of the UV band is around three times larger than at the peak of the visible band (see Fig. S1 the ESI).

PISA spectra for m-DTE$^-$ isomers are shown in Fig. 6b. The PISA spectrum for cycloreversion of ring-closed m-DTE$^-$ resembles the corresponding p-DTE$^-$ PISA spectrum, with a band over the 430–680 nm range, peaking at $\approx$590 nm, and a band of comparable intensity over the 330–420 nm range, peaking at
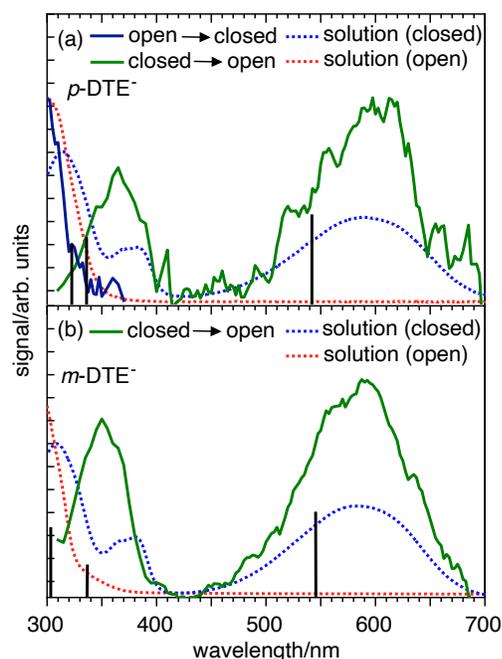
Fig. 6 PISA spectra for isomers of (a) p-DTE$^-$ and (b) m-DTE$^-$. UV-Vis absorption spectra are included for comparison. Black bars indicate vertical excitation wavelengths for the ring-closed isomers calculated using time-dependent density functional theory (TD-DFT) at the ωB97X-D/aug-cc-pVDZ level of theory. UV-Vis absorption spectra were recorded in basic methanol solutions.

$\approx$355 nm. Again, this weaker band is likely a result of two UV transitions that are apparent in the solution absorption spectrum at 367 and 380 nm, respectively. The PISA spectrum is consistent with TD-DFT calculations which predict strong transitions at 545 nm (f=0.43), 335 nm (f=0.21) and 304 nm (f=0.41). As noted above, the ring-open m-DTE$^-$ isomer does not undergo photocyclization. However, its action spectrum recorded on the CO$_2$ loss channel is very similar to the corresponding action spectrum of ring-open p-DTE$^-$ (see Figs. S1 and S2 in the ESI), and is consistent with the predicted UV transition occurring at 268 nm (f=0.16).

Overall, it is apparent from Figs. 4-6 that p-DTE$^-$ and m-DTE$^-$ have very similar photophysical properties, with almost identical absorption band positions in solution and in the gas phase. The one exception is that whereas ring-open p-DTE$^-$ undergoes photocyclisation in the gas phase there is no evidence for corresponding photoisomerisation of ring-open m-DTE$^-$, most likely because the required antiparallel conformation is energetically disfavoured.

Conclusions

Photo-induced 6π-electrocyclisation and cycloreversion reactions of charge-tagged DTE molecules have been probed in the gas phase by combining tandem ion mobility-mass spectrometry and laser excitation. The strategy has enabled us to distinguish the ring-open and ring-closed isomers of DTE molecules in the gas phase and to assess the photoisomerisation responses for the different forms. Whereas reversible photoisomerisation was ob-

served for p-DTE$^-$, only cycloreversion was found for m-DTE$^-$. The absence of 6π-electrocyclisation for the ring-open m-DTE$^-$ isomer can be ascribed to the fact in the gas phase it prefers a parallel structure for which electrocyclisation is not possible. In contrast, both substitutional isomers exhibit reversible photoisomerisation behaviour in methanol.

Preliminary investigations of the photoisomerisation of p-DTE$^-$ and m-DTE$^-$ in solution were also undertaken using ion mobility mass spectrometry to monitor photoisomer formation. The minor ATD peaks that arise when p-DTE$^-$ and m-DTE$^-$ in solution are exposed to 300 nm radiation were tentatively assigned to byproducts. Definite assignment of these peaks requires purification and structural characterisation. Although this is beyond the scope of the current paper, which is mainly concerned with the photoisomerisation of p-DTE$^-$ and m-DTE$^-$ in the gas phase, it may be worthwhile for a future study, particularly given that it may provide the foundation for a rapid on-line protocol for assessing the extent of byproduct formation. The HPLC separation would also allow the UV-Vis spectra of the byproducts from p-DTE$^-$ and m-DTE$^-$ to be measured. Ultimately, a protocol based on ion mobility mass spectrometry may provide a more convenient way for assessing formation of different photoproducts than techniques where product yields are estimated using UV-Vis spectroscopy, given that previous studies for similar DTE molecules show that the byproduct has a very similar absorption spectrum to the ring-closed isomer.[19]

No evidence was found for the formation of the byproduct in the gas phase following exposure of the ring-closed isomers to a single pulse of UV light. Possibly the byproduct would be formed if the gas-phase DTE$^-$ ions were exposed to UV light for longer times. This could perhaps be accomplished by modifying the current instrument so that the ions could be irradiated in the first ion funnel (IF1 in Fig. 2) before the ion packet was launched into the drift region.

Ultimately, we hope this investigation will motivate further studies of DTE-based photoswitches in gas-phase and condensed-phase environments and through quantum chemical methods, and help develop more robust and efficient photoswitches.

Conflicts of interest

There are no conflicts to declare.

Acknowledgements

Notes and references

1 W. R. Browne and B. L. Feringa, *Annu. Rev. Phys. Chem.*, 2009, **60**, 407–428.

2 J. D. Harris, M. J. Moran and I. Aprahamian, *Proc. Natl. Acad. Sci. U.S.A.*, 2018, **115**, 9414–9422.

3 A. A. Beharry and G. A. Woolley, *Chem. Soc. Rev.*, 2011, **40**, 4422–4437.

4 C. Dugave and L. Demange, *Chem. Rev.*, 2003, **103**, 2475–2532.

5 S. Erbas-Cakmak, D. A. Leigh, C. T. McTernan and A. L. Nussbaumer, *Chem. Rev.*, 2015, **115**, 10081–10206.

6 M. Irie, *Chem. Rev.*, 2000, **100**, 1685–1716.

7 M. Irie, T. Fukaminato, K. Matsuda and S. Kobatake, *Chem. Rev.*, 2014, **114**, 12174–12277.

8 S.-Z. Pu, Q. Sun, C.-B. Fan, R.-J. Wang and G. Liu, *J. Mater. Chem. C*, 2016, **4**, 3075–3093.

9 M. Kathan, F. Eisenreich, C. Jurissek, A. Dallmann, J. Gurke and S. Hecht, *Nat. Chem.*, 2018, **10**, 1031–1036.

10 S. Nakamura and M. Irie, *J. Org. Chem.*, 1988, **53**, 6136–6138.

11 K. Uchida, E. Tsuchida, Y. Aoi, S. Nakamura and M. Irie, *Chem. Lett.*, 1999, **28**, 63–64.

12 T. Yamaguchi and M. Irie, *J. Photochem. Photobiol. A: Chem.*, 2006, **178**, 162–169.

13 K. Morimitsu, S. Kobatake, S. Nakamura and M. Irie, *Chem. Lett.*, 2003, **32**, 858–859.

14 K. Morimitsu, S. Kobatake and M. Irie, *Tetrahedron Lett.*, 2004, **45**, 1155–1158.

15 K. Shibata, S. Kobatake and M. Irie, *Chem. Lett.*, 2001, **30**, 618–619.

16 K. Morimitsu, K. Shibata, S. Kobatake and M. Irie, *J. Org. Chem.*, 2002, **67**, 4574–4578.

17 K. Higashiguchi, K. Matsuda, S. Kobatake, T. Yamada, T. Kawai and M. Irie, *Bull. Chem. Soc. Jpn.*, 2000, **73**, 2389–2394.

18 H. Jean-Ruel, R. R. Cooney, M. Gao, C. Lu, M. A. Kochman, C. A. Morrison and R. J. D. Miller, *J. Phys. Chem. A*, 2011, **115**, 13158–13168.

19 M. Irie, T. Lifka, K. Uchida, S. Kobatake and Y. Shindo, *Chem. Commun.*, 1999, 747–750.

20 H. Jean-Ruel, M. Gao, M. A. Kochman, C. Lu, L. C. Liu, R. R. Cooney, C. A. Morrison and R. J. D. Miller, *J. Phys. Chem. B*, 2013, **117**, 15894–15902.

21 S. Kobatake and M. Irie, *Bull. Chem. Soc. Jpn.*, 2004, **77**, 195–210.

22 H. Miyasaka, S. Araki, A. Tabata, T. Nobuto, N. Malaga and M. Irie, *Chem. Phys. Lett.*, 1994, **230**, 249–254.

23 N. Tamai, T. Saika, T. Shimidzu and M. Irie, *J. Phys. Chem.*, 1996, **100**, 4689–4692.

24 H. Miyasaka, T. Nobuto, A. Itaya, N. Tamai and M. Irie, *Chem. Phys. Lett.*, 1997, **269**, 281–285.

25 J. Owrutsky, H. Nelson, A. Baronavski, O.-K. Kim, G. Tsivgoulis, S. Gilat and J.-M. Lehn, *Chem. Phys. Lett.*, 1998, **293**, 555–563.

26 J. Ern, A. Bens, H.-D. Martin, S. Mukamel, D. Schmid, S. Tretiak, E. Tsiper and C. Kryschi, *Chem. Phys.*, 1999, **246**, 115–125.

27 J. Ern, A. Bens, A. Bock, H.-D. Martin and C. Kryschi, *J. Lumin.*, 1998, **76-77**, 90–94.

28 J. Ern, A. Bens, H.-D. Martin, S. Mukamel, D. Schmid, S. Tretiak, E. Tsiper and C. Kryschi, *J. Lumin.*, 2000, **87-89**, 742–744.

29 H. Miyasaka, M. Murakami, A. Itaya, D. Guillaumont, S. Nakamura and M. Irie, *J. Am. Chem. Soc.*, 2001, **123**, 753–754.

30 M. Irie, T. Lifka, S. Kobatake and N. Kato, *J. Am. Chem. Soc.*, 2000, **122**, 4871–4876.

31 P. R. Hania, R. Telesca, L. N. Lucas, A. Pugzlys, J. van Esch, B. L. Feringa, J. G. Snijders and K. Duppen, *J. Phys. Chem. A*, 2002, **106**, 8498–8507.

32 H. Miyasaka, M. Murakami, T. Okada, Y. Nagata, A. Itaya, S. Kobatake and M. Irie, *Chem. Phys. Lett.*, 2003, **371**, 40–48.

33 H. Ikeda, A. Kawabe, A. Sakai, H. Namai and K. Mizuno, *Res. Chem. Intermed.*, 2009, **35**, 893–908.

34 M. Boggio-Pasqua and M. Garavelli, *J. Phys. Chem. A*, 2015, **119**, 6024–6032.

35 M. Isegawa and K. Morokuma, *J. Phys. Chem. A*, 2015, **119**, 4191–4199.

36 I. Hamdi, G. Buntinx, A. Perrier, O. Devos, N. Jaïdane, S. Delbaere, A. K. Tiwari, J. Dubois, M. Takeshita, Y. Wada and S. Aloïse, *Phys. Chem. Chem. Phys.*, 2016, **18**, 28091–28100.

37 I. Hamdi, G. Buntinx, O. Poizat, S. Delbaere, A. Perrier, R. Yamashita, K.-i. Muraoka, M. Takeshita and S. Aloïse, *Phys. Chem. Chem. Phys.*, 2019, **21**, 6407–6414.

38 Y.-T. Wang, Y.-J. Gao, Q. Wang and G. Cui, *J. Phys. Chem. A*, 2017, **121**, 793–802.

39 A. Perrier, S. Aloise, M. Olivucci and D. Jacquemin, *J. Phys. Chem. Lett.*, 2013, **4**, 2190–2196.

40 D. Guillaumont, T. Kobayashi, K. Kanda, H. Miyasaka, K. Uchida, S. Kobatake, K. Shibata, S. Nakamura and M. Irie, *J. Phys. Chem. A*, 2002, **106**, 7222–7227.

41 M. Boggio-Pasqua, M. Ravaglia, M. J. Bearpark, M. Garavelli and M. A. Robb, *J. Phys. Chem. A*, 2003, **107**, 11139–11152.

42 Y. Asano, A. Murakami, T. Kobayashi, A. Goldberg, D. Guillaumont, S. Yabushita, M. Irie and S. Nakamura, *J. Am. Chem. Soc.*, 2004, **126**, 12112–12120.

43 P. D. Patel, I. A. Mikhailov, K. D. Belfield and A. E. Masunov, *Int. J. Quantum Chem.*, 2009, **109**, 3711–3722.

44 D. Mendive-Tapia, A. Perrier, M. J. Bearpark, M. A. Robb, B. Lasorne and D. Jacquemin, *Phys. Chem. Chem. Phys.*, 2014, **16**, 18463–18471.

45 M. Herder, B. M. Schmidt, L. Grubert, M. Pätzel, J. Schwarz and S. Hecht, *J. Am. Chem. Soc.*, 2015, **137**, 2738–2747.

46 J. R. Matis, J. B. Schönborn and P. Saalfrank, *Phys. Chem. Chem. Phys.*, 2015, **17**, 14088–14095.

47 M. V. Oplachko, A. B. Smolentsev, I. M. Magin, I. P. Pozdnyakov, V. A. Nichiporenko, V. P. Grivin, V. F. Plyusnin, V. V. Vyazovkin, V. V. Yanshole, M. V. Parkhats, A. V. Yadykov, V. Z.

Shirinian and E. M. Glebov, *Phys. Chem. Chem. Phys.*, 2020, **22**, 5220–5228.

48 A. Goldberg, A. Murakami, K. Kanda, T. Kobayashi, S. Nakamura, K. Uchida, H. Sekiya, T. Fukaminato, T. Kawai, S. Kobatake and M. Irie, *J. Phys. Chem. A*, 2003, **107**, 4982–4988.

49 S. Nakamura, T. Kobayashi, A. Takata, K. Uchida, Y. Asano, A. Murakami, A. Goldberg, D. Guillaumont, S. Yokojima, S. Kobatake and M. Irie, *J. Phys. Org. Chem.*, 2007, **20**, 821–829.

50 T. Sumi, Y. Takagi, A. Yagi, M. Morimoto and M. Irie, *Chem. Commun.*, 2014, **50**, 3928–3930.

51 M. Hanazawa, R. Sumiya, Y. Horikawa and M. Irie, *J. Chem. Soc., Chem. Commun.*, 1992, 206–207.

52 Y.-C. Jeong, S. I. Yang, E. Kim and K.-H. Ahn, *Tetrahedron*, 2006, **62**, 5855–5861.

53 N. Tanaka, C. Okabe, K. Sakota, T. Fukaminato, T. Kawai, M. Irie, A. Goldberg, S. Nakamura and H. Sekiya, *J. Mol. Struct.*, 2002, **616**, 113–118.

54 A. Lietard, G. Piani, L. Poisson, B. Soep, J.-M. Mestdagh, S. Aloïse, A. Perrier, D. Jacquemin and M. Takeshita, *Phys. Chem. Chem. Phys.*, 2014, **16**, 22262–22272.

55 N. J. A. Coughlan, K. J. Catani, B. D. Adamson, U. Wille and E. J. Bieske, *J. Chem. Phys.*, 2014, **140**, 164307.

56 N. Coughlan, B. Adamson, L. Gamon, K. Catani and E. Bieske, *Phys. Chem. Chem. Phys.*, 2015, **17**, 22623–22631.

57 J. N. Bull, M. S. Scholz, E. Carrascosa, G. da Silva and E. J. Bieske, *Phys. Rev. Lett.*, 2018, **120**, 223002.

58 M. S. Scholz, J. N. Bull, E. Carrascosa, B. D. Adamson, G. K. Kosgei, J. J. Rack and E. J. Bieske, *Inorg. Chem.*, 2018, **57**, 5701–5706.

59 J. N. Bull, E. Carrascosa, N. Mallo, M. S. Scholz, G. da Silva, J. E. Beves and E. J. Bieske, *J. Phys. Chem. Lett.*, 2018, **9**, 665–671.

60 J. N. Bull, G. d. Silva, M. S. Scholz, E. Carrascosa and E. J. Bieske, *J. Phys. Chem. A*, 2019, **123**, 4419–4430.

61 B. D. Adamson, N. J. A. Coughlan, R. E. Continetti and E. J. Bieske, *Phys. Chem. Chem. Phys.*, 2013, **15**, 9540–9548.

62 B. D. Adamson, N. J. A. Coughlan, P. B. Markworth, R. E. Continetti and E. J. Bieske, *Rev. Sci. Instrum.*, 2014, **85**, 123109.

63 J. N. Bull, E. Carrascosa, L. Giacomozzi, E. J. Bieske and M. H. Stockett, *Phys. Chem. Chem. Phys.*, 2018, **20**, 19672–19681.

64 M. J. Frisch, G. W. Trucks, H. B. Schlegel, G. E. Scuseria, M. A. Robb, J. R. Cheeseman, G. Scalmani, V. Barone, G. A. Petersson, H. Nakatsuji, X. Li, M. Caricato, A. V. Marenich, J. Bloino, B. G. Janesko, R. Gomperts, B. Mennucci, H. P. Hratchian, J. V. Ortiz, A. F. Izmaylov, J. L. Sonnenberg, D. Williams-Young, F. Ding, F. Lipparini, F. Egidi, J. Goings, B. Peng, A. Petrone, T. Henderson, D. Ranasinghe, V. G. Zakrzewski, J. Gao, N. Rega, G. Zheng, W. Liang, M. Hada, M. Ehara, K. Toyota, R. Fukuda, J. Hasegawa, M. Ishida, T. Nakajima, Y. Honda, O. Kitao, H. Nakai, T. Vreven, K. Throssell, J. A. Montgomery, Jr., J. E. Peralta, F. Ogliaro, M. J. Bearpark, J. J. Heyd, E. N. Brothers, K. N. Kudin, V. N. Staroverov, T. A. Keith, R. Kobayashi, J. Normand, K. Raghavachari, A. P. Rendell, J. C. Burant, S. S. Iyengar, J. Tomasi, M. Cossi, J. M. Millam, M. Klene, C. Adamo, R. Cammi, J. W. Ochterski, R. L. Martin, K. Morokuma, O. Farkas, J. B. Foresman and D. J. Fox, *Gaussian 16 Revision B.01*, 2016, Gaussian Inc. Wallingford CT.

65 J.-D. Chai and M. Head-Gordon, *Phys. Chem. Chem. Phys.*, 2008, **10**, 6615–6620.

66 T. H. Dunning Jr., *J. Chem. Phys.*, 1989, **90**, 1007–1023.

67 V. Shrivastav, M. Nahin, C. J. Hogan and C. Larriba-Andaluz, *J. Am. Soc. Mass Spectrom.*, 2017, **28**, 1540–1551.

68 B. H. Besler, K. M. Merz Jr. and P. A. Kollman, *J. Comput. Chem.*, 1990, **11**, 431–439.

69 U. C. Singh and P. A. Kollman, *J. Comput. Chem.*, 1984, **5**, 129–145.

70 S. Poyer, C. Comby-Zerbino, C. M. Choi, L. MacAleese, C. Deo, N. Bogliotti, J. Xie, J.-Y. Salpin, P. Dugourd and F. Chirot, *Anal. Chem.*, 2017, **89**, 4230–4237.

Physical Chemistry Chemical Physics Accepted Manuscript